Numerical study for performance-based design of piled raft with grid-form DMWs under large earthquake load

Yoshimasa Shigeno, Kiyoshi Yamashita & Junji Hamada
Takenaka Research & Development Institute, Takenaka Corporation, Inzai, Chiba, Japan

ABSTRACT
Seismic performance of a piled raft foundation with grid-form deep mixing walls (DMWs) in soft ground under large earthquake loads is evaluated numerically. A base-isolated building located in Tokyo is modeled as a detailed three-dimensional finite element ground–structure interaction model. This model has been verified through the numerical simulation using the medium seismic motion recorded at the site during the 2011 off the Pacific Coast of Tohoku Earthquake in the previous study. The base input motions, that are officially notified for a performance design in Japanese building design codes, are used as large earthquake loads. A nonlinear model with tensile and shear criteria is applied for the stabilized soil. Numerical cases without the grid-form DMWs are also analyzed to clarify an effect of the DMWs on the pile behavior. Based on the analysis results, the maximum bending moment of the piles in the cases without the DMWs is markedly large. It is beyond the allowable structural capacity of the pile, and very close to the ultimate capacity in some cases. In contrast, although the induced stress in the DMWs partially reached the tensile strength, the maximum bending moment in the case with the grid-form DMWs is below the allowable structural capacity. Thus, the grid-form DMWs are found to be quite effective at reducing the sectional force of the piles to an acceptable level under large earthquake loads, even if partial failure occurs in the DMWs. Consequently, piled rafts with the grid-form DMWs could be designed more rationally following the principles of performance-based design (PBD) in which a partial failure of the DMWs is accepted under the performance level required.

1 INTRODUCTION

In recent years, the effectiveness of piled rafts at reducing average and differential settlements has been confirmed on soft clay and even on liquefiable sand with grid-form cement deep mixing walls (DMWs) (Yamashita et al., 2011, 2013, 2016). The grid-form DMWs work not only as a countermeasure of liquefaction to increase the resistance of unstabilized soil but also as a resistance component against the horizontal load. However, adding the grid-form DMWs to a piled raft as a new component, the seismic behavior becomes more complicated and the necessity for detailed evaluation increases to develop more reliable design methods, particularly in highly active seismic areas such as Japan.

To investigate the seismic response of a piled raft foundation with grid-form DMWs, the field monitoring has been performed on the piled raft system in soft ground supporting a 12-story building, and the seismic response of the soil-foundation system was successfully recorded at the time of the 2011 off the Pacific coast of Tohoku Earthquake (Yamashita et al., 2012). Targeting these observation records, the seismic response analysis using a detailed three-dimensional finite element model with equivalent linear moduli was conducted, and the analytical results agreed well with the observation records (Hamada et al., 2014). Seismic analysis using nonlinear soil model was also conducted, and the more suitable deformation parameters were determined to simulate the observation records more accurately for the improved soil as well as the unimproved soil (Shigeno et al., 2016).

In this paper, the dynamic analyses using two large earthquake motions for performance design in Japan are conducted. Through the analyses, the effects of the inertial force and dynamic earth pressure on the DMWs and the piles are investigated, and the effectiveness of the grid-form DMWs on reducing the sectional force of the piles is discussed according to the design concept of performance-based design (PBD).

2 BUILDING AND GROUND CONDITION

Figure 1 shows a schematic view of the building and its foundation with the soil profile. The building analyzed is a 12-story residential building located in Tokyo. The soil down to a depth of 44m is alluvial stratum. The soil profile

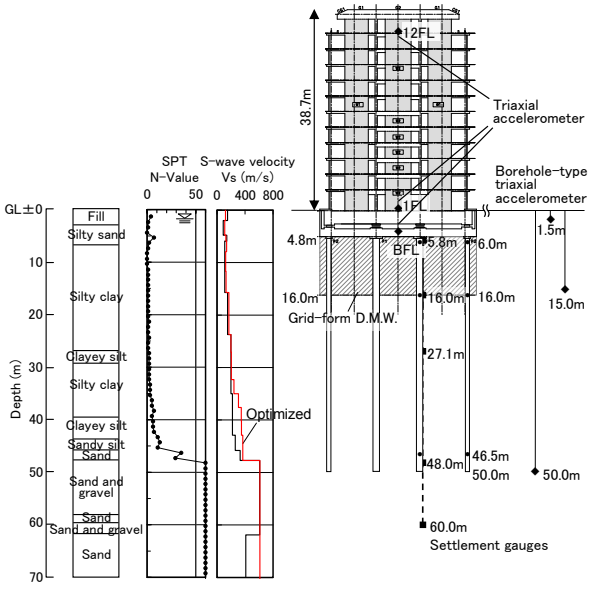

Figure 1. Schematic view of building foundation with soil profile

down to the depth of 7m is made of fill, soft silt and loose silty sand where the ground water table appears approximately 1.8 m below the ground surface. The piled raft with grid-form DMWs that are employed to prevent liquefaction of the silty sand from GL -3 m to -7 m as well as to improve the bearing capacity of the raft foundation supports the building. The soil conditions, the foundation design and the instrumentation, as well as the seismic response of the soil-foundation-structure system, were reported by Yamashita et al. (2012) in detail.

2.1 Finite Element Model

Figure 2 shows the finite element (FE) mesh. The superstructure is modeled using elastic bar and shells, and the piles are modeled using elastic bar. Table 1 shows the dimensions and material properties of the piles. The raft is modeled using elastic solid elements with the modulus of concrete. Rayleigh damping is applied to these components at a damping ratio of 2%. Modeling of the soil and the DMWs is described later in detail.

Figure 3 shows a top view of the FE mesh beneath the raft and the foundation plan. The spacing between the DMWs is about 6 to 9 m. To consider the shape and volume of the piles, cavities in the shape of the piles are made. The nodes of the piles and the adjacent ground nodes at the same depth are bound by rigid bars. The

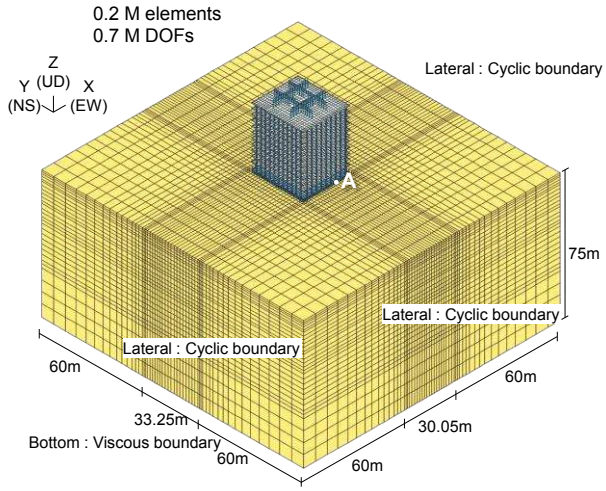

Figure 2. FE mesh of ground–structure interaction model

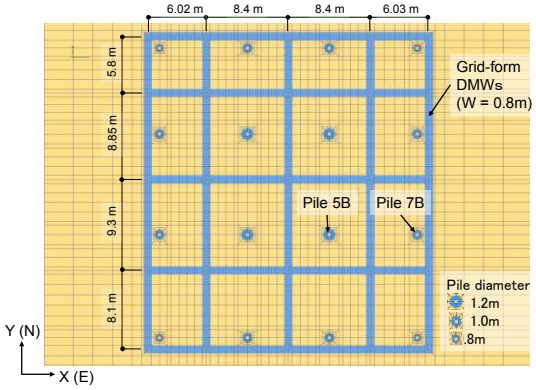

Figure 3. Top view of FE mesh for piles and grid-form DMWs

base isolation system is modeled using a tri-linear spring (Hamada et al., 2014). The lateral boundaries are periodic boundaries, and are positioned 60 m outside of the building to reduce the boundary effect. The bottom is a viscous boundary at a depth of 75 m from the ground surface. The software is an in-house program called MuDIAN (Shiomi et al., 1993). It is parallelized using the hybrid parallel method and is able to analyze a large-DOF model at high speed (Shigeno et al., 2014).

Table 1 Material characteristics of piles

Pile diameter	(mm)	800	1000	1200
Young's modulus	(MN/m^2)	40000	40000	40000
Damping	(%)	2	2	2
Ae of SC pile	(m^2)	0.3268	0.4649	0.6714
Ie of SC pile	(m^4)	0.02199	0.04899	0.10316
Ae of PHC pile	(m^2)	0.2441	0.3633	0.5054
Ie of PHC pile	(m^4)	0.01455	0.03437	0.06958

Ae : Equivalent cross-sectional area, Ie : Equivalent moment of inertia of area

2.2 Input Motions

Large earthquakes have been chosen from level 2 waves that are officially notified in Japanese design code. Level 2 waves are used for the performance design of a building. The waves are defined as the response spectrum and generated using phase data. In this paper, the Kobe phase data and the Hachinohe phase data are used. The Kobe phase data were observed at the Kobe Marine Observatory during the 1995 Hyogoken-Nambu earthquake (referred as the Kobe phase hereafter). The Hachinohe phase data were recorded at Tokachi - Oki Earthquake (1968) at Hachinohe Bay (referred as the Hachinohe phase hereafter). Figure 4 shows the input accelerations in the NS direction at the bedrock (the waves are 2E). The time interval is 0.005 s and the analysis time is 120 s. Figure 5 shows the acceleration response spectrum of the input waves.

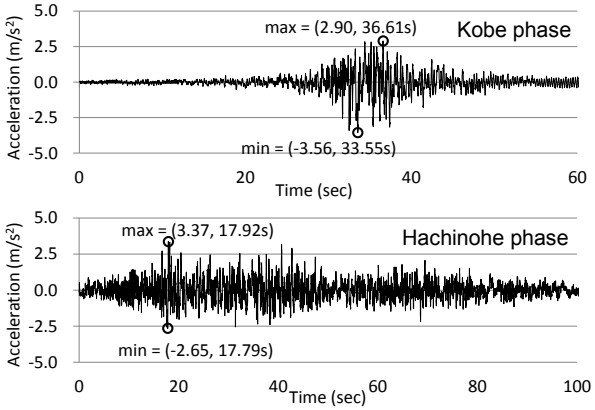

Figure 4. Input motions at a depth of 75 m (2E)

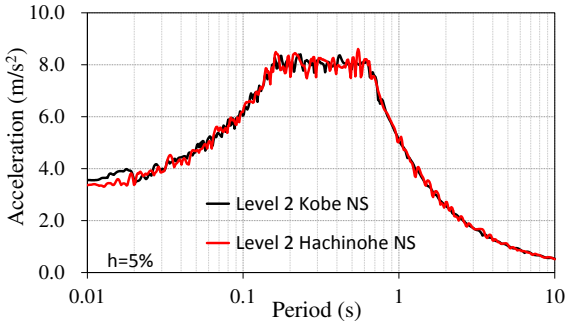

Figure 5. Acceleration response spectrum of input motions

2.3 Constitutive Model and Properties of Soil

The Yoshida model for multi-dimension (Tsujino et al., 1994) is used as the constitutive model for the soil. The Yoshida model is a multi-surface nonlinear elastic model and is characterized using shear modulus and shear strain (G-γ) and damping and shear strain (h-γ) characteristics directly as input data.

The profile of shear wave velocity of the ground for the analysis is shown in Figure 1 together with data derived from P-S logging. The profile of shear wave velocity was obtained by the optimization method using the P-S logging results and the observation records of the small earthquakes (Hamada et al., 2014). The G-γ and h-γ relations of each soil layer are shown in Figure 6. The other soil properties are reported in Shigeno et al. 2016. Initial damping other than the damping induced by the constitutive model is assumed 1%, and is given by Rayleigh damping.

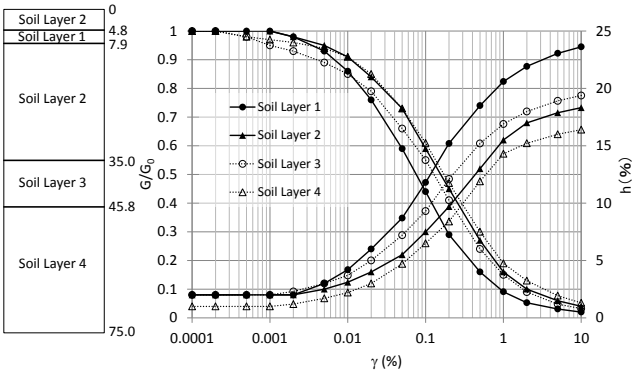

Figure 6. Strain dependent characteristics of soil

2.4 Constitutive Model and Properties of Stabilized Soil

The failure of the DMWs is caused by tension or shear. Both the tensile and shear criteria have to be used to evaluate the correct strength. The Hayashi–Hibino model (Motojima et al., 1978) is used as a two criteria model in this study. The Hayashi–Hibino model is a nonlinear elastic model that is able to evaluate tensile and shear failure, and the elastic modulus reduces to the user specified value at failure. This model is also able to express nonlinearity before failure using the proximity ratio to the criteria *R*. The elastic moduli are reduced according to *R* in the following equations using the nonlinear parameter *a*.

$$E = R^{1/a} E_0, \quad 0.45 - \nu = R^{1/2a}(0.45 - \nu_0) \qquad [1]$$

where E is Young's modulus, ν is Poisson's ratio, and subscripted with 0 is the initial value of each.

The design standard compressive strength F_c is used as the compressive strength of the stabilized soil. The value of F_c is calculated using the average compressive strength of in-situ core samples q_{uf} and its coefficient of variation V_{quf} referred to BCJ (2002) as follows.

$$F_c = (1 - 1.3V_{q_{uf}})q_{uf} \qquad [2]$$

The value of q_{uf} and V_{quf} are 3.8 MPa and 0.25 that are the average and variance of 36 core samples aged 28 days (Yamashita et al., 2015), and the value of F_c becomes 2.6 MPa. The tensile strength and the cohesion are 0.2 and 0.3 times the compressive strength respectively quoted from Namikawa (2007). The friction angle and the Poisson's ratio are assumed to be 30 degrees and 0.26 referred to BCJ (2002).

The nonlinear parameter '*a*' is obtained by simulating simple shear test to fit the G-γ curve reported by Kuroda et al. (2001) as shown in Figure 7. Damping of the stabilized soil is needed because the model is nonlinear elastic. The damping ratio is assumed to be 5% also referred to Kuroda et al. (2001).

As for the initial stress in the DMWs, isotropic stress of 170 kPa is given by considering the measured vertical pressure between the raft and the DMWs of 300 kPa (Yamashita et al., 2015) and the horizontal stress calculated using the coefficient of earth pressure at rest.

The initial shear modulus (G_0 = 500 MPa) was determined based on the nonlinear analysis targeting the observation records of the 2011 off the Pacific Coast Tohoku Earthquake (Shigeno et al., 2016). The analytical results agreed well with the observations, especially with the bending moment near the pile heads with this modulus.

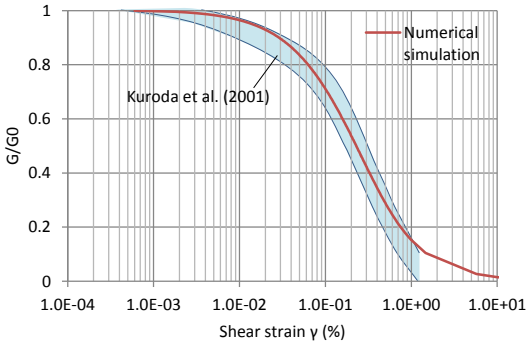

Figure 7. Strain dependent characteristic of stabilized soil

3 RESULTS OF SEISMIC RESPONSE ANALYSES

The case without DMWs is analysed to clarify the effect of them in each input motion, then totally four analysis cases are examined as listed in Table 2.

Table 2 Numerical cases

Case	Input motion	DMWs
K1	Kobe phase	Yes
K2	Kobe phase	No
H1	Hachinohe phase	Yes
H2	Hachinohe phase	No

3.1 Response of Ground and Structure

Figure 8 shows the profiles of the peak horizontal acceleration at the center of the superstructure and the raft in the NS direction together with those of the ground at point A (Figure 2). The response of the soil column model is also shown denoted as “Free field”.

The maximum ground surface acceleration at the free field is 3.33 m/s^2 under Kobe phase motion, and 2.95 m/s^2 under Hachinohe phase motion. The responses at the raft top (GL-4.8 m) are slightly smaller than the free field in all cases due to the input loss.

In Case K1 (with DMWs), the acceleration peaks are 2.57 m/s^2 at the raft and 1.46 m/s^2 on the first floor. This reduction is due to the base isolation system. In Case K2 (without DMWs), the peaks are 2.83 m/s^2 and 1.29 m/s^2 respectively. The peak acceleration at the raft in Case K1 is smaller than that in Case K2. This may be attributed to the input loss due to existence of the DMWs.

In Case H1 (with DMWs), the peaks are 2.65 m/s^2 at the raft and 1.31 m/s^2 on the first floor, the reduction rate is 49%, and in Case H2 (without DMWs), the peaks were 2.76 m/s^2 and 1.11 m/s^2. The input loss by the DMWs is also seen between the two.

Figure 9 shows the profiles of the peak horizontal relative displacement to the depth of 49.9 m at the center of the superstructure and the ground at point A in the NS direction. It is seen that the ground displacements above the bottom of the DMWs in the cases with DMWs are considerably smaller than those in the cases without DMWs. The maximum displacements are reduced to about 70%. This indicates that the ground deformation is significantly reduced by the DMWs.

Figure 10 shows the profiles of the peak bending moment in piles 5B and 7B, shown in Figure 3, in the NS direction. The peak bending moments near the pile head in the cases with DMWs is remarkably smaller than those in the cases without DMWs. It is also seen that the bending moments near pile head in Case K2 are fairly larger than those in Case H2 while in Case K1 are similar to those in Case H1, which suggests that the bending moments near pile head in the cases with DMWs would be less affected by the input motions. From Figure 9 and 10, it is seen that the deformation of the soil enclosed by the grid-form DMWs is reduced, and that results in the decrease of the bending moment near the pile head.

3.2 Lateral Resistance of Piled Raft System against Large Earthquake Loads

Mechanism of lateral resistance of the piled raft system against large earthquake is investigated using the results

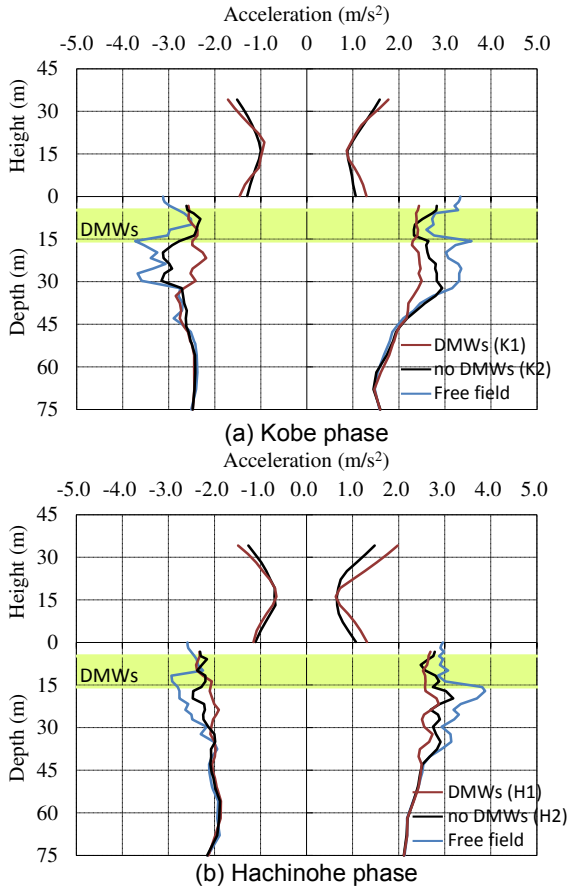

Figure 8. Peak acceleration profiles of superstructure at center, ground at point A and free-field

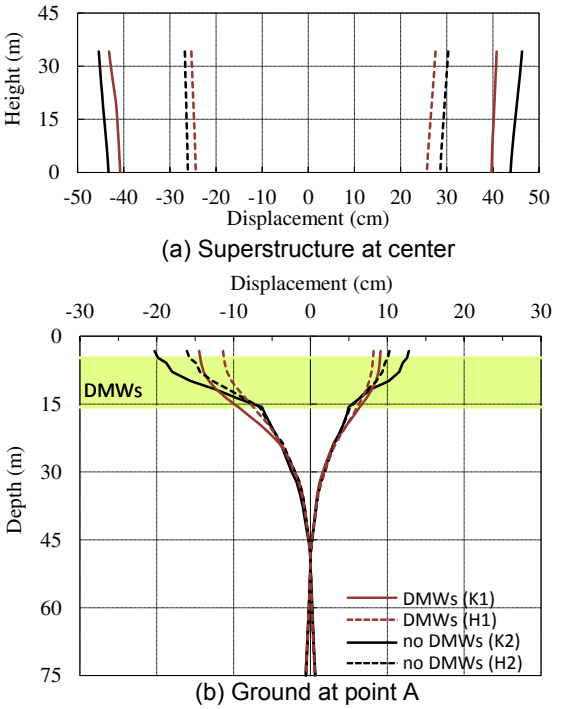

Figure 9. Peak displacement profiles of superstructure at center and ground at point A

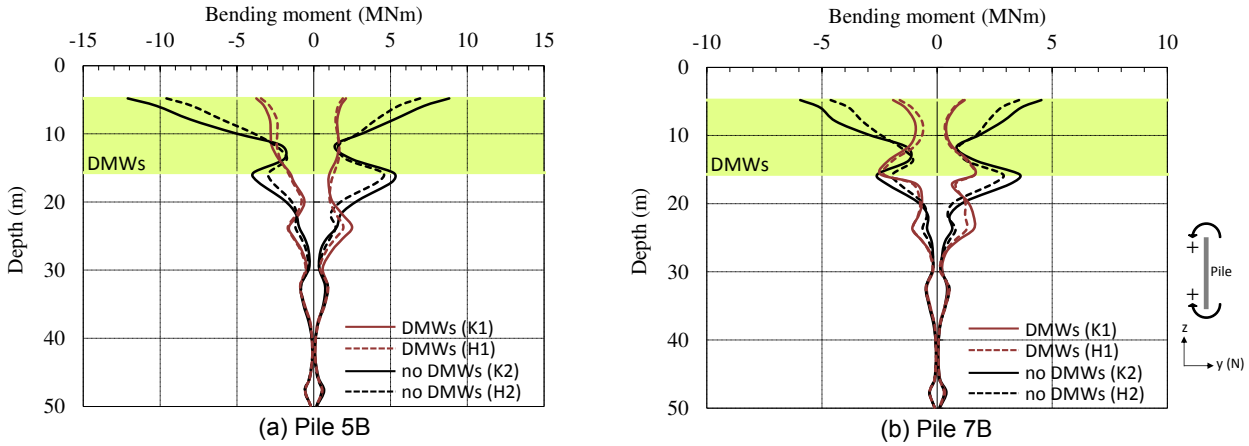

(a) Pile 5B (b) Pile 7B

Figure 10. Profiles of peak bending moment in Piles 5B and 7B

of Case K1 (with DMWs) and K2 (without DMWs). Figure 11(a) shows the time histories of the lateral external forces acting on the bottom surface of the raft during the time of 32-39 s when the response of the building is large. The external forces consist of the inertial forces from the superstructure and the raft as well as the earth pressure induced by ground movements acting on the sides of the buried raft. In both the cases, the peak value of the earth pressure is significantly large in comparison with the other two. It is also seen that the peak value of the earth pressure in Case K1 is larger than that in Case K2.

Figure 11(b) shows the time histories of the lateral resistance forces of the foundation elements acting on the bottom surface of the raft. The resistance forces are the shear force of the piles at the pile head and that of the soil beneath the raft as well as the shear force of the grid-form DMWs. In Case K1 (with DMWs), it is seen that the shear force of the grid-form DMWs is significantly larger than those of the piles and the soil, and the shear force of the piles is quite small. On the other hand, the shear force of the piles is the same level compared to that of the soil in Case K2 (without DMWs).

Figure 12 illustrates the equilibrium of lateral force at the level of the raft bottom in the shaking direction when the total external force reached the peak values in each case. In Case K1, the dynamic earth pressure from the ground corresponded to about 77% of the total external force. The dynamic earth pressure is canceled entirely with the shear force of the DMWs which carries 82% of the lateral force. In contrast, the shear force of the piles is very small while 15% of the lateral force is carried by the soil. In Case K2, the dynamic earth pressure corresponded to 70% of the lateral force, and is carried by the piles and the soil evenly. Under Hachinohe wave, the lateral force and the ratio of force sharing among the foundation elements show the same tendency.

3.3 Deformation and Partial Failure in DMWs

As shown in Figure 11 and 12, a significant part of the lateral load is carried by the grid-form DMWs, then the induced internal stresses in the DMWs should be examined against their ultimate capacity for the PBD of this combined type piled raft system. Figure 13 illustrates

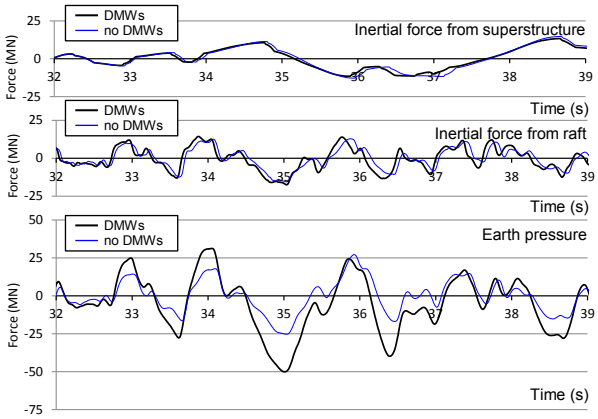

(a) Lateral force from the structure

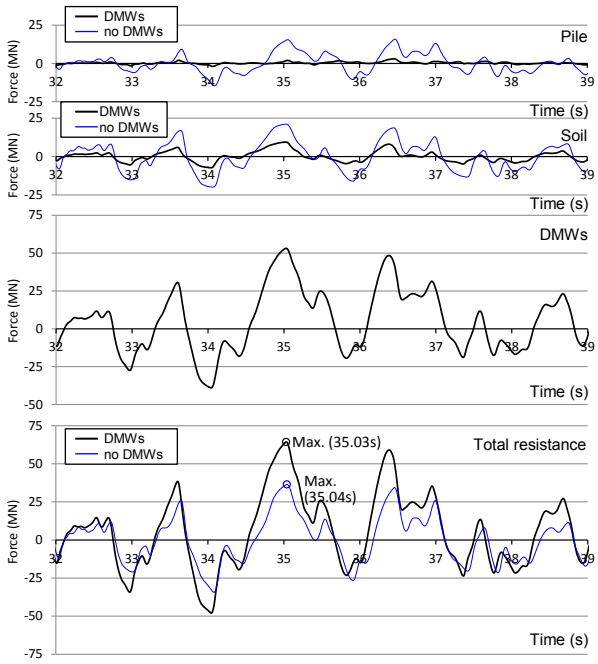

(b) Lateral resistance

Figure 11. Time histories of lateral force and resistance at the raft bottom, Kobe phase

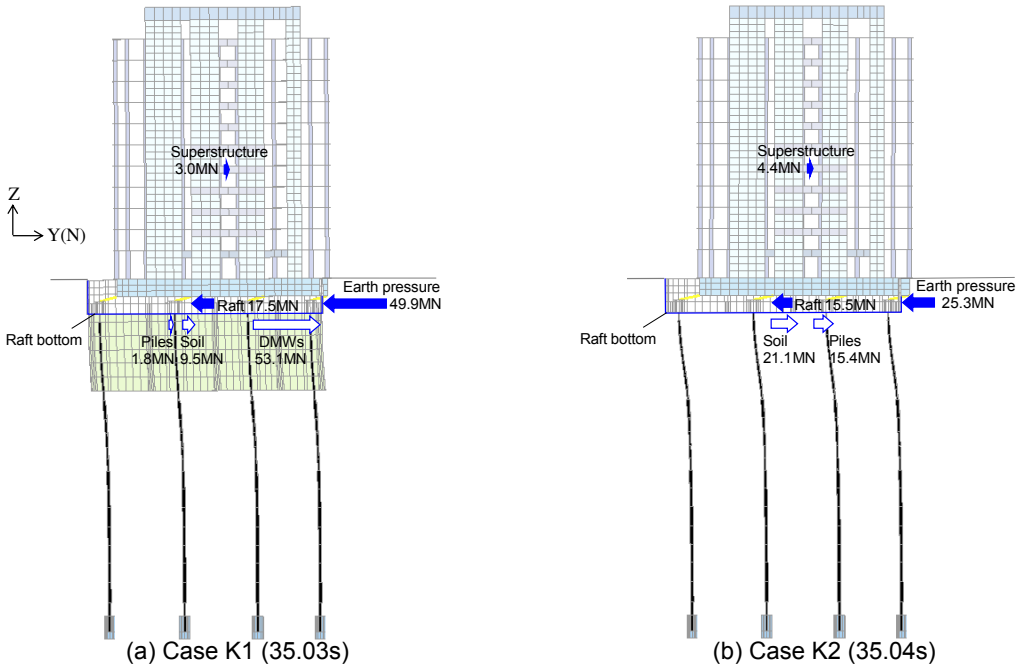

(a) Case K1 (35.03s) (b) Case K2 (35.04s)

Figure 12. Equilibrium of lateral force at the raft bottom, Kobe phase (deformation is enlarged by 10 times)

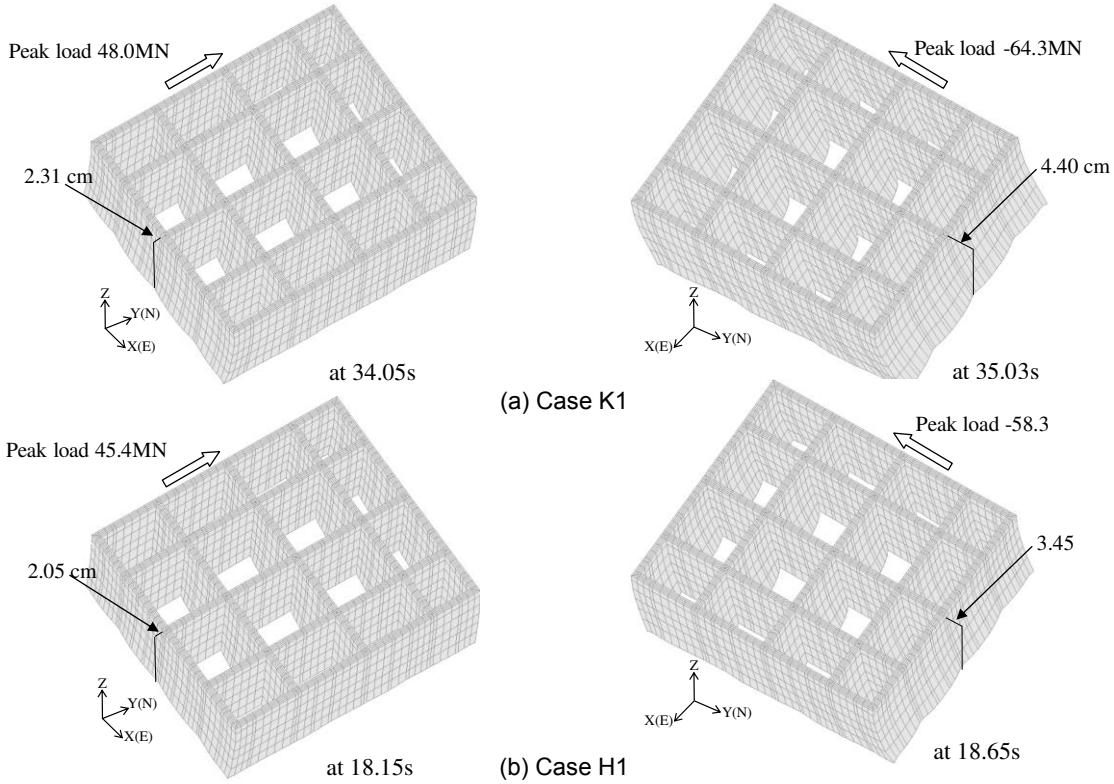

Figure 13. Deformation of DMWs at the time when peak external force occurred

the deformation mode of the grid-form DMWs in K1 and H1 at the time when the peak lateral load from the structure occurred. The shear deformation of the longitudinal walls in Case K1 is larger than that in Case H1. In addition, the displacements at the mid-length of the transverse walls in both the cases showed significant flexure due to bending, but little flexure near the top of them.

Figure 14 illustrates the extent of tensile failure in the grid-form DMWs in Cases K1 and H1 during the earthquake. Elements are colored according to the number of Gauss points which tensile failure occurs.

Number of Gauss points is eight in each element. It is seen that the tensile failure is very limited, and the degree of tensile failure is large in Case H1 than in Case K1. Thus, the failure behavior is clearly affected by the input motion. The tensile failure is seen mostly in the longitudinal walls, and this is due to shear. In the transverse walls, a few failure elements are seen at the bottom of grid crossing corners due to bending, though the elements of which all the Gauss points fail are very limited.

Figure 15 shows the extent of shear failure in the grid-form DMWs. The maximum number of shear failure Gauss points is four in Case H1. The degree of shear failure is much smaller than that of tensile failure. This shows the DMWs fail mainly by tension. The degree of shear failure is also larger in Case H1, and no shear failure elements are seen in Case K1. The shear failure is also affected by the input motion. Figure 15 also shows that top surface of the DMWs does not fail by shear. This means that sliding between the top surface of the DMWs and the bottom surface of the raft does not occur.

Although the constitutive model used in the present analysis does not consider softening of the stabilized soil after the failure (Namikawa et al., 2007), the analysis results would be acceptable in the engineering point of view because the extent of failure in the DMWs is very limited as shown in Figure 14 and 15.

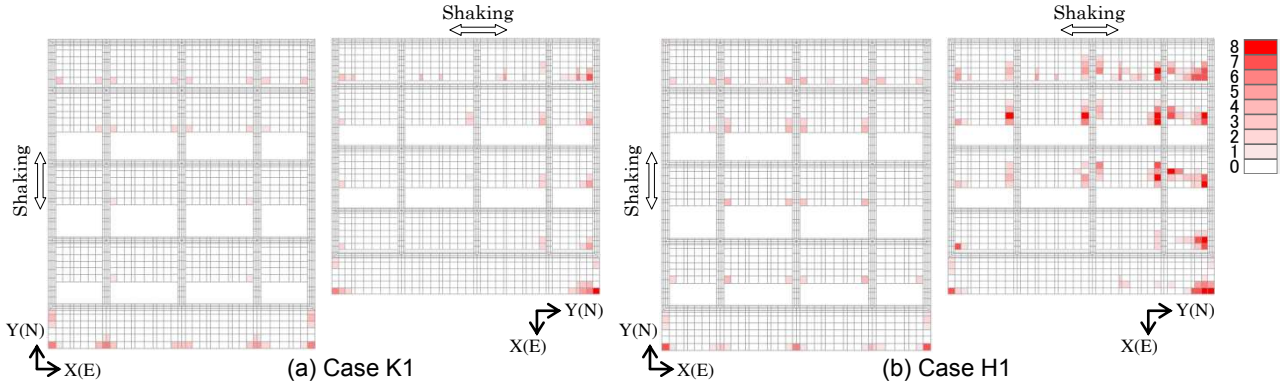

(a) Case K1 (b) Case H1

Figure 14. Tensile failure Gauss points in grid-form DMWs

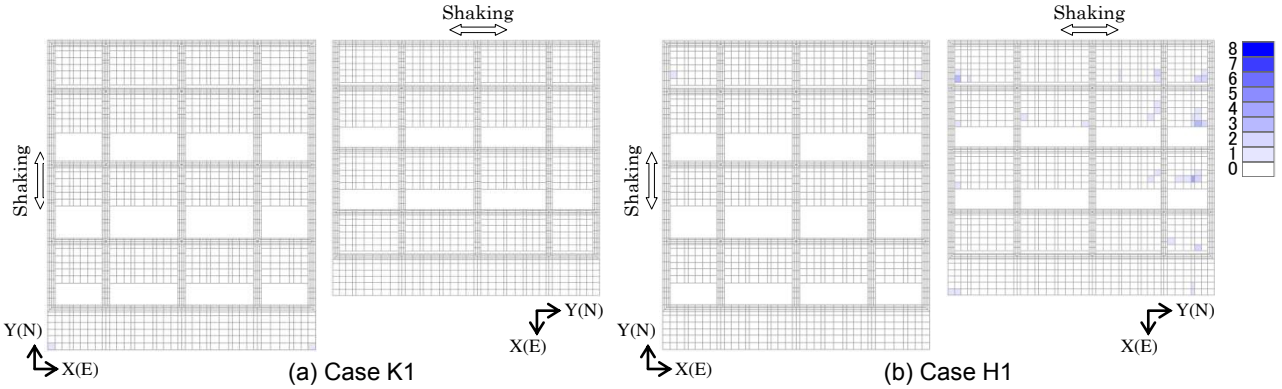

(a) Case K1 (b) Case H1

Figure 15. Shear failure Gauss points in grid-form DMWs

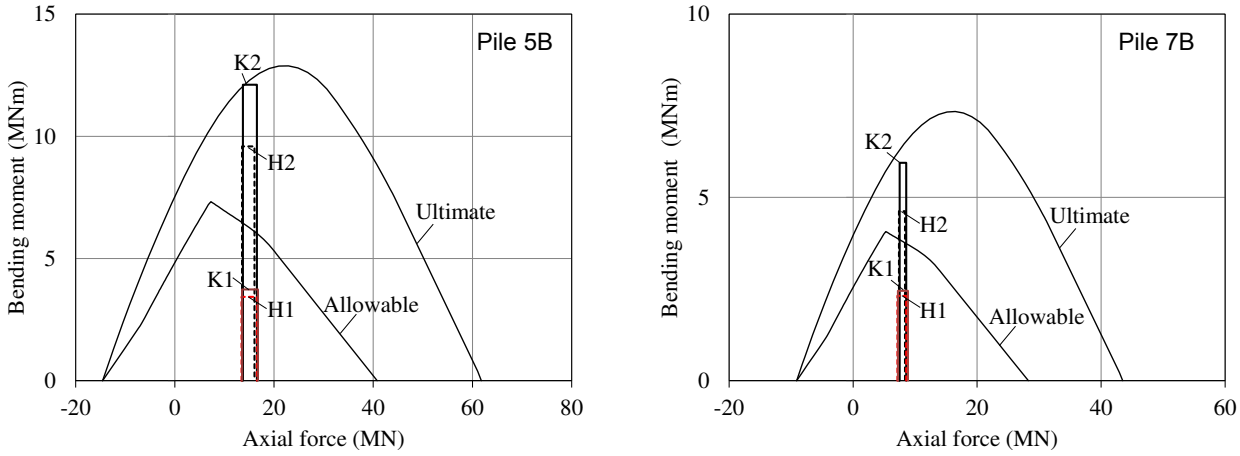

Figure 16. Calculated maximum moment along pile and design NM-interaction curves of SC piles

3.4 Verification of Induced Bending Moment of Piles

Figure 16 shows the relationship between the axial force and the bending moment of piles 5B and 7B, together with the design interaction curves of the steel pipe–concrete composite (SC) pile (which is used in the top portion at 12 m). Here, the axial force means the sum of the statically measured pile head load and the peak dynamic increments in the analyses, and the bending moment means the maximum value along the SC pile in the NS direction. The analysis results show that the maximum bending moments in Case K1 and H1 are well below the allowable criterion (the unit stress at the edge of the concrete is in the elastic condition). In contrast, the maximum bending moments in Case K2 and H2 are fairly beyond the allowable criterion and in Case K2, they are nearly equal to the ultimate criterion (the unit stress at the edge of the concrete reaches the compressive strength). Hence, the grid-form DMWs are quite effective at reducing pile bending moment to an acceptable level, although the induced stress in the DMWs partially reached the tensile strength under large earthquakes. This indicates that the grid-form DMWs can be designed more rationally by accepting a partial failure of the DMWs as pointed out by Namikawa et al. (2007). The analysis results also suggest that the 3D FE simulation employed in this study can provide adequate solutions for the PBD of piled rafts with the grid-form DMWs.

4 CONCLUSION

Through the dynamic simulation analyses, the following conclusions can be drawn.

(1) Comparing by the existence of the DMWs, the peak ground displacements near the surface are considerably small, and the peak bending moment of the piles near the pile head are significantly small in the case with DMWs.
(2) Tensile failure occurred in the DMWs but very limited. The tensile failure is seen mostly in the longitudinal walls. This suggests that the lateral load from the structure is carried mainly by the longitudinal walls. As is seen that the extent of failure in Case H1 is larger than Case K1, the failure behavior is affected by the input motion. On the other hand, almost no shear failure occurs in the DMWs.
(3) The maximum bending moments along the pile in the cases with DMWs are considerably below the allowable criterion of the design NM relation of the piles, while those in the case without DMWs are markedly large. This arises because the lateral ground movements below the raft are significantly reduced by the DMWs and the lateral load from the structure is carried mostly by the DMWs. Thus, the grid-form DMWs are found to be quite effective at reducing the sectional force of piles to an acceptable level, even if partial failure occurs in the DMWs.
(4) The DMWs can be regarded as supplementary structural elements in the foundation. Therefore, minor damages to the DMWs could be tolerated providing that the required performance is satisfied. Consequently, piled rafts with the grid-form DMWs could be designed more rationally following the principles of PBD in which a partial failure is accepted under the performance level required.

REFERENCES

Building Center of Japan, 2002. *Specification for design and quality control of cement treated soil* (in Japanese).

Hamada, J., Shigeno, Y., Onimaru, S., Tanikawa, T., Nakamura, N. and Yamashita, K. 2014. Numerical analysis on seismic response of piled raft foundation with ground improvement based on seismic observation records, *The 14th IACMAG*, Kyoto, Japan.

Kuroda, T., Tanaka, H., Tomii, Y. and Suzuki, Y. 2001. Evaluation of characteristics of improved soil by deep mixing method of soil stabilization, *2001 Summaries of Technical Papers of Annual Meeting of AIJ (Kanto)*, Tokyo, Japan, 699-700 (in Japanese).

Motojima, M., Hibino, S. and Hayashi, M. 1978. Development of computer program for stability analysis of excavation, *Central Research Institute of Electric Power Industry Report*, 377012 (in Japanese).

Namikawa, T., Koseki, J. and Suzuki, Y. 2007. Finite element analysis of lattice-shaped ground improvement by cement-mixing for liquefaction mitigation, *Soils & Foundations*, Vol.47, 559-576.

Shigeno, Y., Hamada, J. and Nakamura, N. 2014. Hybrid parallelization of earthquake response analysis using K computer, *The 14th IACMAG*. Kyoto, Japan.

Shigeno, Y., Yamashita, K. and Hamada, J. 2016. Seismic Performance of Piled Raft Foundation with Grid-Form DMWs under Large Earthquake Load, *Takenaka Technical Research Report*, No.72, 37-49.

Shiomi, T., Shigeno, Y. and Zienkiewicz, O. C. 1993. Numerical prediction for model No. 1., *Verification of Numerical Procedures for the Analysis of Soil Liquefaction Problems*, Balkema, 213-219.

Tsujino, S., Yoshida, N. and Yasuda, S. 1994. A simplified practical stress-strain model in multi-dimensional analysis, *International Symposium on Pre-failure Deformation Characteristics of geomaterials*, Sapporo, Japan, 463-468.

Yamashita, K., Yamada, T., and Hamada, J. 2011. Investigation of settlement and load sharing on piled rafts by monitoring full-scale structures, *Soils & Foundations,* Vol. 51 (3), 513–532.

Yamashita, K., Hamada, J., Onimaru, S. and Higashino, M. 2012. Seismic behavior of piled raft with ground improvement supporting a base-isolated building on soft ground in Tokyo, *Soils & Foundations*, Vol. 52, 1000–1015.

Yamashita, K., Wakai, S. and Hamada, J. 2013. Large-scale piled raft with grid-form deep mixing walls on soft ground, *Proc. of the 18th Int. Conference on SMGE*, Paris, France, 2637-2640.

Yamashita, K., Tanikawa, T., Shigeno, Y. and Hamada, J. 2015. Vertical load sharing of piled raft with grid-form deep mixing walls, *Conference on Deep Mixing 2015*, San Francisco, USA, 437-446.

Yamashita, K., Hamada, J. and Tanikawa, T. 2016. Static and seismic performance of a friction piled combined with grid-form deep mixing walls in soft ground, *Soils & Foundations*, Vol. 56, 559-573.